




Frustrated magnetism in the J1 - J2 honeycomb lattice compounds MgMnO₃ and ZnMnO₃ synthesized via a metathesis reaction

著者	Yuya Haraguchi, Kazuhiro Nawa, Chishiro Michioka, Hiroaki Ueda, Akira Matsuo, Koichi Kindo, Maxim Avdeev, Taku J Sato, Kazuyoshi Yoshimura
journal or publication title	Physical Review Materials
volume	3
number	12
page range	124406
year	2019-12-17
URL	http://hdl.handle.net/10097/00128337

doi: 10.1103/PhysRevMaterials.3.124406

Frustrated magnetism in the J_1 - J_2 honeycomb lattice compounds MgMnO_3 and ZnMnO_3 synthesized via a metathesis reaction

Yuya Haraguchi ^{1,*}, Kazuhiro Nawa ^{2,†}, Chishihiro Michioka,¹ Hiroaki Ueda,¹ Akira Matsuo,³ Koichi Kindo,³ Maxim Avdeev ^{4,5}, Taku J. Sato,² and Kazuyoshi Yoshimura^{1,6,7,8}

¹Department of Chemistry, Graduate School of Science, Kyoto University, Kyoto 606-8502, Japan

²Institute of Multidisciplinary Research for Advanced Materials, Tohoku University, 2-1-1 Katahira, Sendai 980-8577, Japan

³The Institute for Solid State Physics, The University of Tokyo, Kashiwa, Chiba 277-8581, Japan

⁴Australian Nuclear Science and Technology Organisation, Kirrawee DC, NSW 2232, Australia

⁵School of Chemistry, The University of Sydney, Sydney 2006, Australia

⁶Research Center for Low Temperature and Materials Sciences, Kyoto University, Kyoto 606-8502, Japan

⁷International Research Unit of Integrated Complex System Science, Kyoto University, Kyoto 606-8501, Japan

⁸International Research Unit of Advanced Future Studies, Kyoto University, Kyoto 606-8502, Japan



(Received 27 August 2019; revised manuscript received 6 November 2019; published 17 December 2019)

We investigated the magnetic properties of the ilmenite-type manganates MgMnO_3 and ZnMnO_3 , both of which are composed of a honeycomb lattice of magnetic Mn^{4+} ions. Both compounds show antiferromagnetic order with weak ferromagnetic moments. In particular, MgMnO_3 exhibits a magnetization “reversal” behavior which can be described by the N -type ferrimagnetism in the Néel’s classification. The relationship between the magnetic properties and the crystal and magnetic structures probed by the neutron diffraction experiments indicates that the two honeycomb lattice magnets have different J_1 - J_2 parameter sets, placing them in the distinct regions in the phase diagram; both nearest neighbor (NN) and next nearest neighbor (NNN) exchange interactions are antiferromagnetic in MgMnO_3 , while NN and NNN interactions become ferromagnetic and antiferromagnetic, respectively, in ZnMnO_3 .

DOI: [10.1103/PhysRevMaterials.3.124406](https://doi.org/10.1103/PhysRevMaterials.3.124406)

I. INTRODUCTION

Frustrated magnets have attracted much attention for their ground states and excitations [1–4]. A spin frustration is realized in a characteristic geometrical spin arrangement based on a regular triangle, such as triangular and kagome lattices. On the other hand, in square and honeycomb lattice antiferromagnets, the nearest neighbor interactions J_1 do not compete, and thus they often exhibit a Néel order. Even in these antiferromagnets, competition of magnetic interactions can be induced by next nearest neighbor interactions J_2 , leading to an exotic ground state. From this viewpoint, the most interesting system would be the J_1 - J_2 honeycomb lattice magnets. For $J_2/J_1 > \frac{1}{6}$ with antiferromagnetic J_1 and J_2 , it is theoretically predicted that the ground state is highly degenerate [5], which results in exotic spin liquids characterized by “ring” or “pancake”-like structure factors [6]. In addition, exotic multiple- q magnetic order can occur in the parameter range of $\frac{1}{6} < J_2/J_1 < \frac{1}{2}$ [7,8]. However, few candidates are regarded as the J_1 - J_2 honeycomb lattice model compounds. One candidate is nitrated bismuth manganate $\text{Bi}_3\text{Mn}_4\text{O}_{12}(\text{NO}_3)$, where competition of antiferromagnetic J_1 and J_2 ($\sim 0.1 J_1$) is present [9,10]. This

compound does not show a long-range magnetic order down to 0.4 K despite a relatively large Weiss constant of -257 K [9]. Neutron scattering and muon spin resonance experiments, respectively, detect the development of short-range order [11] and spin glass-like anomaly at 6 K [12]. For the honeycomb lattice magnet with ferromagnetic J_1 and antiferromagnetic J_2 , no candidate compound has been found so far.

Antiferromagnets formed by d^3 ions should be a rich playground to investigate the frustrated magnetism. This is because nearest neighbor magnetic couplings J_1 between d^3 ions on edge-sharing MO_6 octahedra (M transition metal) consist of two components: superexchange interactions J_s and direct exchange interactions J_d . The opposite signs of J_s and J_d result in relatively small J_1 . On the other hand, usually next nearest neighbor couplings J_2 are dominated by super-superexchanges, which are not so strong. As a result, a large degeneracy can be induced by comparable J_1 and J_2 . Therefore, searching a magnetic material with a honeycomb lattice formed by d^3 ions (for example, Mn^{4+} or Cr^{3+}) should be meaningful to explore exotic magnetic states.

The J_1 - J_2 honeycomb magnets have been found in some ilmenite-type compounds [13–16], whose chemical formula is given by ABO_3 . Their crystal structure is shown in Fig. 1. AO_6 (BO_6) octahedra share their edges forming a two-dimensional honeycomb layer, and the two layers are alternately stacked to share faces of octahedra along the c axis with mutual shifting. The ilmenite-type compounds $\text{MgMn}^{4+}\text{O}_3$ and $\text{ZnMn}^{4+}\text{O}_3$

*Present address: Department of Applied Physics, Tokyo University of Agriculture and Technology, Koganei, Tokyo 184-8588, Japan; chiyuya3@go.tuat.ac.jp

†knawa@tohoku.ac.jp

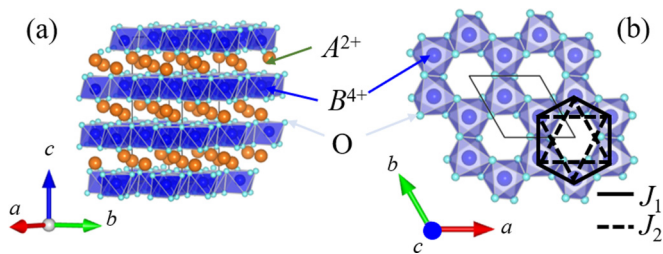


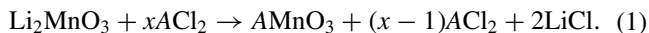
FIG. 1. Crystal structure of ilmenite-type structure $A^{2+}B^{4+}O_3$ (a) viewed along the c axis and (b) perpendicular to the ab plane with magnetic pathways J_1 and J_2 in a honeycomb layer drawn by solid and broken lines. The VESTA program is used for visualization [17].

have a potential to be good model compounds of J_1 - J_2 honeycomb lattice antiferromagnets. Their basic magnetic properties were reported by Chamberland *et al.* [15]. However, detailed magnetic properties, especially those below T_N , and crystal structures have not been investigated.

We report their magnetic properties, and crystal and magnetic structures, and discuss their relationship in terms of the J_1 - J_2 honeycomb lattice model. Interestingly, a spin model of $ZnMnO_3$ is well described by a J_1 - J_2 honeycomb system with ferromagnetic J_1 and antiferromagnetic J_2 .

II. EXPERIMENTAL METHODS

We found that $MgMnO_3/ZnMnO_3$ can be synthesized alternatively via a metathetical reaction between Li_2MnO_3 and $ZnCl_2/MgCl_2$ salts. A precursor material Li_2MnO_3 was prepared by the conventional solid-state reaction method according to the previous report [18]. The obtained precursors were ground well with an excess of ACl_2 ($A = Mg, Zn$) in an Ar-filled glove box, sealed in an evacuated silica tube, and then heated at 400 °C for 100 h. The metathesis reaction is expressed as



The unreacted starting material ACl_2 and the byproduct $LiCl$ were removed by washing the sample with distilled water. The obtained polycrystalline samples were characterized by powder neutron diffraction using high-resolution powder diffractometer Echidna. Neutrons with wavelength $\lambda = 1.6220$ Å were selected by a monochromator using the Ge 335 reflections for room-temperature scans. In addition, to investigate magnetic structures, low-temperature scans were performed by using a wavelength of 2.4395 Å monochromated by the Ge 331 reflections. The temperature was controlled by a top-loading cryostat between 4 and 60 K. Vanadium cans were used as a sample container. Rietveld analyses were conducted by the FULLPROF suite [19].

The temperature dependence of the magnetization of powder samples was measured under several magnetic fields up to 7 T by using a magnetic property measurement system (MPMS, Quantum Design) equipped at the LTM Research Center, Kyoto University. In order to prevent particle re-orientation by the magnetic field, the powder samples were tightly compacted in the sample holder. The temperature dependence of the specific heat of pressed powder samples was measured by using a conventional relaxation method with

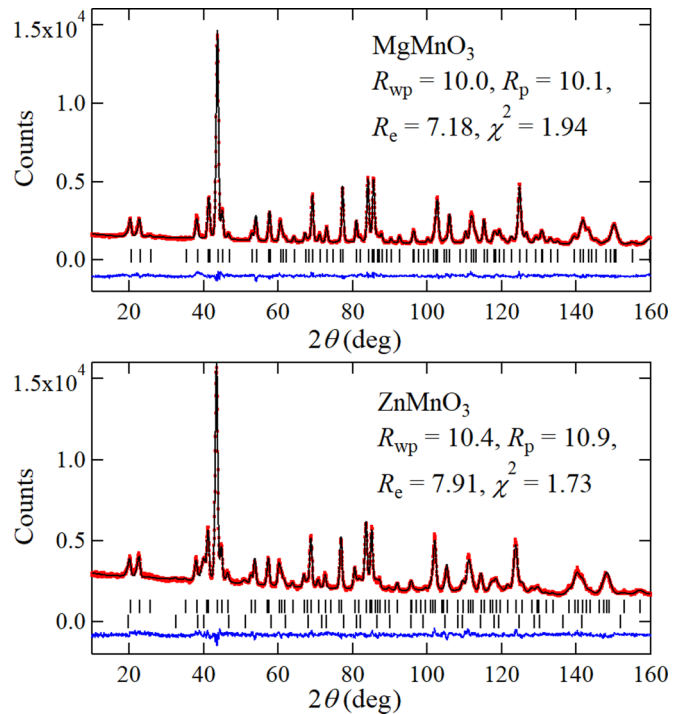


FIG. 2. Powder neutron diffraction patterns of $MgMnO_3$ and $ZnMnO_3$ at room temperature (plotted by red dots). Total neutron counts are $4.0(3.9) \times 10^5$ for $MgMnO_3$ ($ZnMnO_3$). Black vertical bars indicate positions of Bragg reflections. For $ZnMnO_3$, the Bragg reflections from the main and secondary phases are indicated by top and bottom vertical bars, respectively. Solid black and blue curves indicate the results of Rietveld analysis and the difference between observed and calculated data, respectively.

a physical property measurement system (PPMS, Quantum Design). Magnetization measurements up to about 75 T were performed using an induction method with a multilayer pulse magnet at the Ultrahigh Magnetic Field Laboratory of the Institute for Solid State Physics at the University of Tokyo.

III. RESULTS

A. Crystal structure

Powder neutron diffraction patterns of $MgMnO_3$ and $ZnMnO_3$ are shown in Fig. 2. For both compounds, all the peaks except for those from impurity peaks can be indexed by the ilmenite-type structure with the space group of $R\bar{3}$. As shown in Figs. 1(a) and 1(b), Mn ions form a regular honeycomb lattice in the ilmenite structure. The structures of $MgMnO_3$ and $ZnMnO_3$ were refined by using the Rietveld method as described in the experimental section. For $ZnMnO_3$, 11 wt % of $Li_2Zn_{1-\delta}Mn_{3+\delta}O_8$ ($Fd\bar{3}m$) is detected as a secondary phase. The details of the refinement parameters are given in Table I. The bond valence sum calculation for Mn ions yields +3.91 and +4.09, respectively, for $MgMnO_3$ and $ZnMnO_3$, which are consistent with the expected valence of +4.

The bond distances and bond angles strongly affect the magnitude of the nearest neighbor exchange interactions, as we discuss later. The nearest neighbor Mn-Mn bond distances

TABLE I. Crystallographic parameters for MgMnO_3 and ZnMnO_3 (both $R\bar{3}$) determined from powder neutron diffraction experiments. The obtained lattice parameters are $a = 4.9430(2)$, $c = 13.7249(5)$ Å and $a = 4.9650(3)$, $c = 13.7850(7)$ Å, respectively, for MgMnO_3 and ZnMnO_3 . B is the atomic displacement parameter.

	Site	x	y	z	B (Å ²)
MgMnO₃					
Mg	6c	0	0	0.35998(13)	0.472(29)
Mn	6c	0	0	0.15831(17)	0.105(31)
O	18f	0.34879(25)	0.04051(16)	0.08903(6)	0.302(20)
ZnMnO₃					
Zn	6c	0	0	0.36584(19)	0.434(34)
Mn	6c	0	0	0.15914(23)	0.126(43)
O	18f	0.32011(35)	0.02838(24)	0.24352(9)	0.266(26)

are 2.8630(4) and 2.8741(5) Å, respectively, for MgMnO_3 and ZnMnO_3 . The bond distances are comparable to the other Mn oxides, such as 2.870(3) Å for honeycomb lattice $\text{Bi}_3\text{Mn}_4\text{O}_{12}(\text{NO}_3)$ [9], 2.8963(8) Å for ordered spinel $\text{Li}_2\text{ZnMn}_3\text{O}_8$ [20], and 2.826–2.851 Å for maple-leaf lattice $\text{MgMn}_3\text{O}_7 \cdot 3\text{H}_2\text{O}$ [21], all of which consist of edge-sharing Mn^{4+}O_6 octahedra. On the other hand, the Mn-O-Mn bond angles, which correspond to exchange path between nearest neighbor Mn ions (J_1), are found as 97.47(5)° for MgMnO_3 and 98.14(6)° for ZnMnO_3 .

B. Magnetic properties

The temperature dependences of magnetic susceptibility χ for powder samples of MgMnO_3 and ZnMnO_3 are shown in Fig. 3. As shown in the inset, $1/\chi$ has a linear relation-

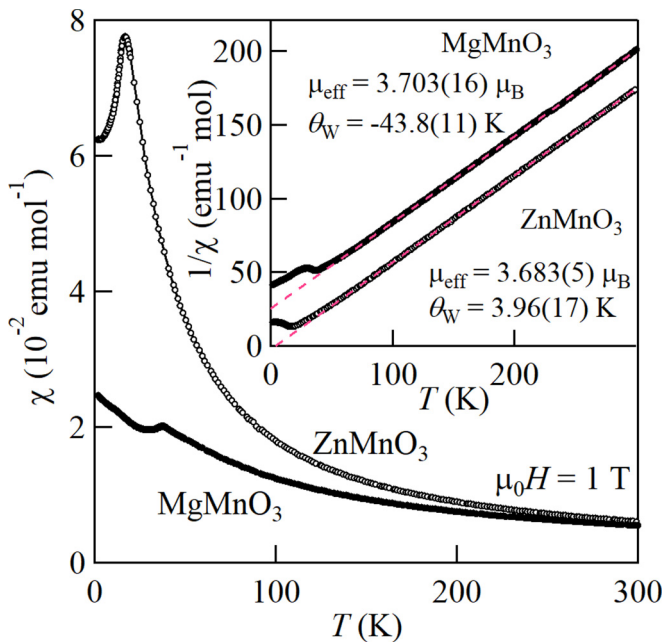


FIG. 3. Temperature dependences of magnetic susceptibility χ of powder samples of MgMnO_3 and ZnMnO_3 measured under 1 T. The inverse magnetic susceptibility $1/\chi$ is shown in the inset. The dashed lines indicate the Curie-Weiss fit in the high-temperature region. The μ_{eff} and θ_{W} in the inset indicate the effective magnetic moment and the Weiss temperature determined from the fit, respectively.

ship with T at high temperatures. The Curie-Weiss fitting with the range between 200 and 300 K yields the effective paramagnetic moment $\mu_{\text{eff}} = 3.703(16)\mu_{\text{B}}$ with the Weiss temperature $\theta_{\text{W}} = -43.8(11)$ K for MgMnO_3 , and $\mu_{\text{eff}} = 3.683(5)\mu_{\text{B}}$ with $\theta_{\text{W}} = 3.96(17)$ K for ZnMnO_3 . The estimated μ_{eff} for both compounds is in good agreement with the spin-only value of $3.87\mu_{\text{B}}$ expected for $S = 3/2$. In addition, the estimated θ_{W} is close to those in the previous report [15]. Remarkably, the magnitudes of θ_{W} for both compounds are considerably different from each other. At low temperatures, a single peak is observed in χ , indicating antiferromagnetic order. The magnetic transition temperature T_{N} is estimated as 37.9 and 17.4 K, respectively, for MgMnO_3 and ZnMnO_3 from the peak position.

In Fig. 4, the M/H of ZnMnO_3 measured under various magnetic fields are plotted as a function of T . At 1 T, M/H simply decreases below T_{N} . In contrast, below 0.1 T, M/H starts to increase above T_{N} , and saturates below T_{N} as the temperature is decreased. In addition, a thermal hysteresis appears between the zero-field-cooled (ZFC) and field-cooled (FC) data. With increasing the magnetic field, the increase of M/H is suppressed. Furthermore, as shown in the inset,

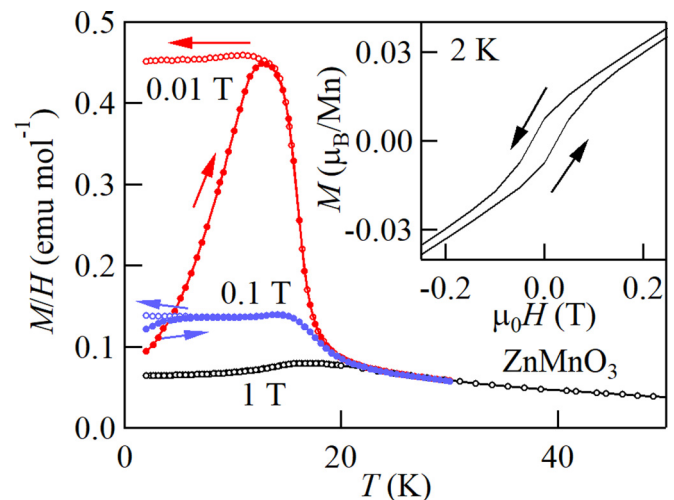


FIG. 4. The temperature dependence of the magnetization divided by the magnetic field M/H for a powder sample of ZnMnO_3 measured at several magnetic fields. The inset shows the isothermal magnetization curve at 2 K.

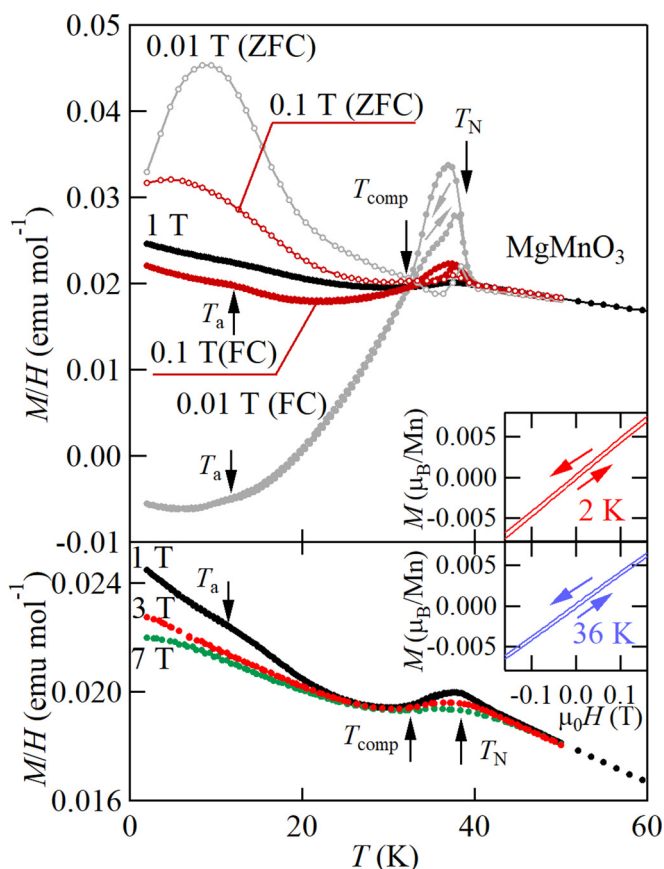


FIG. 5. The temperature dependence of the magnetization divided by the magnetic field M/H for a powder sample of MgMnO_3 measured at several magnetic fields. The top and bottom panels show the M/H measured below 1 T, and above 1 T, respectively. The insets show the enlarged view of the magnetization curve near zero field measured at 2 and 36 K.

a magnetic hysteresis loop in the M - H curve is observed at 2 K. These magnetic properties demonstrate the presence of a weak ferromagnetic moment likely due to a canted antiferromagnetic order. Due to the presence of magnetic impurity $\text{Li}_2\text{Zn}_{1-\delta}\text{Mn}_{3+\delta}\text{O}_8$ [22,23], it is difficult to estimate the magnitude of the weak ferromagnetic moment. However, the presence of the weak ferromagnetic moment should be intrinsic since the magnitude of a weak ferromagnetic moment does not differ so much for three differently prepared samples (see Supplemental Material [24]).

The M/H of MgMnO_3 exhibits different temperature dependence compared with ZnMnO_3 , as shown in Fig. 5. The M/H under FC starts to increase above T_N , and shows a sharp increase at T_N . Then it decreases with decreasing temperature, and finally reaches negative if the magnetic field is very small. On the other hand, M/H under ZFC increases again and remains positive at low temperatures. Note that M/H under ZFC is larger than that of FC below 30 K, while this relation is reversed above 30 K. This magnetization “reversal” is observed only below 0.1 T. Above 1 T, the peak at T_N and the increase below 30 K are still present, whereas the increase of M/H becomes smaller. The temperature dependence cannot be explained by that of a canted antiferromagnet, where M/H

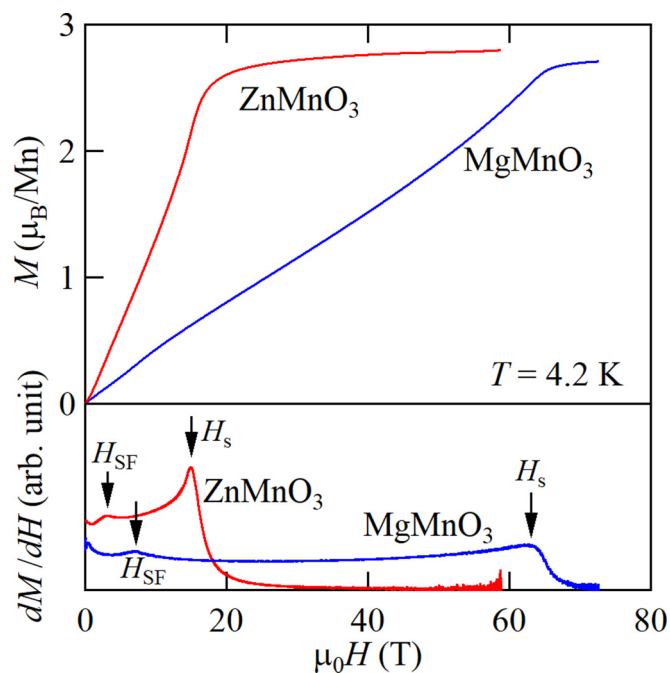


FIG. 6. Magnetization M (top panel) and field derivative of magnetization dM/dH (bottom panel) at $T = 4.2$ K. H_{SF} and H_s indicate the spin-flop and magnetic saturation fields, respectively.

would just increase and saturate as the temperature is lowered. The temperature dependence is consistent with that expected for a very weak N -type ferrimagnet in the Néel’s classification [25]. In an N -type ferrimagnet, there are a few magnetic sublattices which have sufficiently different temperature dependence from each other. As a result, the spontaneous magnetization changes sign with changing temperature. The presence of a compensation point T_{comp} , where ZFC and FC curves cross, supports the occurrence of an N -type ferrimagnetic order. Such an unconventional behavior in magnetization after FC is attributed to freezing of the magnetic domain wall movement at T_N where the weak-ferromagnetic component is positive along the external field, while it is negative at low temperatures. In addition, the magnetization curves both at 2 K (below T_{comp}) and 36 K (above T_{comp} and below T_N) show very small spontaneous magnetization with hysteresis, indicating the presence of a ferromagnetic moment as shown in the upper inset. Note that only one equivalent site of Mn atoms is present in MgMnO_3 . This is in contradiction with the ferrimagnetic order, which requires more than two inequivalent sites. The crystal symmetry may be lowered as we discuss later.

C. High-field magnetization

Figure 6 shows magnetization curves up to 75 T at 4.2 K. Both curves show anomalies at 7.0 and 2.9 T for powder samples of MgMnO_3 and ZnMnO_3 , respectively. In the dM/dH curves, the anomalies are observed as small peaks. These anomalies should correspond to spin-flop transitions, since both compounds exhibit collinear antiferromagnetic order, as revealed by neutron diffraction experiments. As the magnetic field is increased, magnetization curves saturate at 63.0 and

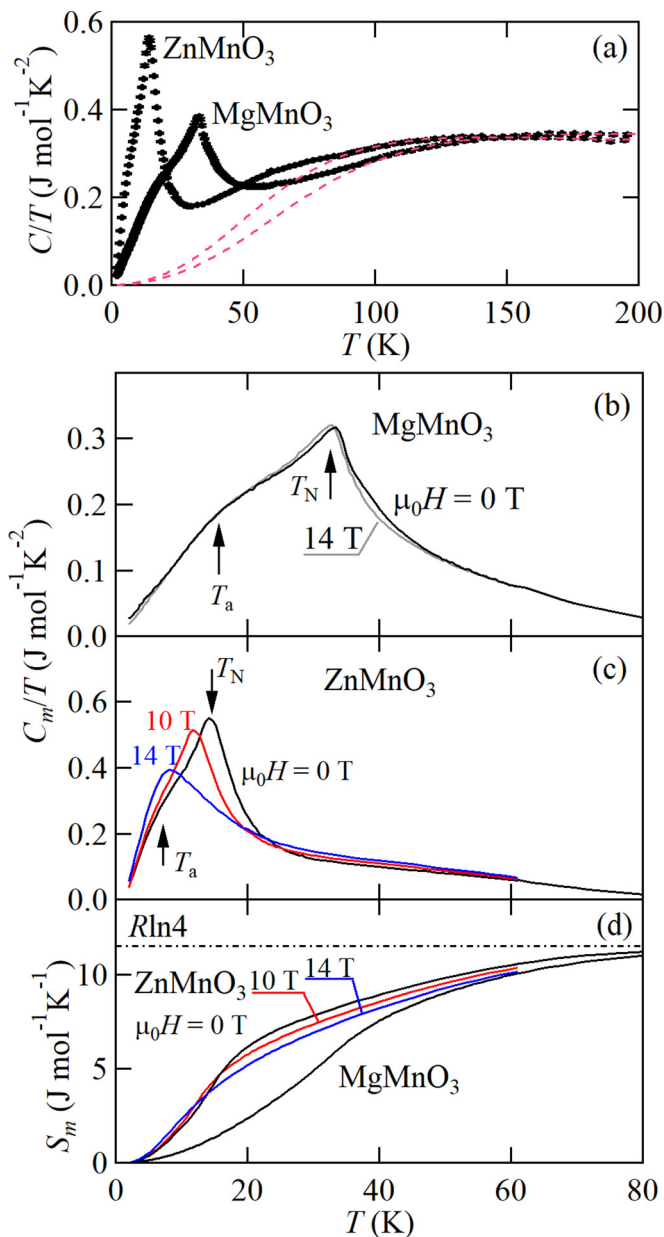


FIG. 7. (a) Temperature dependence of the heat capacity divided by temperature C/T for MgMnO₃ and ZnMnO₃. The dashed lines represent the lattice contribution estimated by fitting the data above 100 K, as described in the text. Temperature dependence of magnetic heat capacity divided by temperature C_m/T of (b) MgMnO₃ and (c) ZnMnO₃ under several fields. (d) The magnetic entropy S_m of MgMnO₃ and ZnMnO₃ obtained by integrating C_m/T as a function of temperature.

14.9 T, respectively, for MgMnO₃ and ZnMnO₃. The full moment is close to $3 \mu_B$, as expected for Mn⁴⁺ ions.

D. Thermodynamic properties

The result of heat capacity measurements supports the presence of the magnetic transition. Figure 7(a) shows the temperature dependence of the heat capacity divided by temperature C/T for the pressed powder samples of MgMnO₃ and ZnMnO₃. To extract the magnetic contribution to the

heat capacity, the lattice contribution was estimated by fitting the high-temperature part where the magnetic heat capacity may be negligible. Provided that they are the sum of Debye- and Einstein-type heat capacities, C_D and C_E , respectively, the C/T data above 100 K are fitted to the equation $C/T = 3R\{aC_D/T + (5-a)C_E/T\}$, where R is the gas constant and a is the weight parameter. The best fits are shown by the dashed line with $a = 1.18(3)$ and $1.09(4)$, Debye temperature $\theta_D = 542(8)$ and $449(6)$ K, and Einstein temperature $\theta_E = 1274(39)$ and $1161(54)$ K, respectively, for MgMnO₃ and ZnMnO₃. The magnetic contribution was obtained by subtracting this lattice contribution from the experimental data. The temperature dependences of the magnetic heat capacity divided by the temperature C_m/T are shown in Figs. 7(b) and 7(c). The C_m/T of both compounds exhibits similar temperature dependence. The C_m/T exhibits a lambda-type anomaly at T_N , indicating the occurrence of magnetic order.

In addition, at zero field, a shoulder is present at $T_a = 17$ and 7 K for MgMnO₃ and ZnMnO₃, respectively. Such broad shoulder suggests that magnetic order is not complete at T_N , and remaining magnetic entropy is released around T_a . Similar anomalies have been observed in other frustrated magnets such as NaCrO₂ [26], KCu₃As₂O₇(OH)₃ [27], and RbCr₂F₆ [28]. The shoulder at T_a can also be due to the same origin, though details still remain unclear. For ZnMnO₃, it is difficult to determine whether the anomaly at T_a is intrinsic or not, owing to the presence of magnetic impurities. However, since sample dependence was again found to be small, we think that the entropy release at T_a is likely to be intrinsic.

E. Neutron diffraction experiments

In order to clarify the difference of magnetism between MgMnO₃ and ZnMnO₃, we performed the neutron diffraction studies. The neutron diffraction pattern of MgMnO₃ at 3 and 60 K is shown in Fig. 8(a). While observed peaks at 60 K are well indexed by nuclear reflections, intensities of some reflections increase below T_N , indicating the occurrence of a $q = 0$ magnetic order.

On the other hand, in the case of ZnMnO₃, new Bragg peaks appear below T_N as shown in Fig. 9(a). The neutron diffraction pattern at 40 K shows nuclear reflections from ZnMnO₃, Li₂Zn_{1- δ} Mn_{3+ δ} O₈ [22], and several unindexed peaks at 2θ ranges of 76.1° – 79.6° , 89.6° – 91.0° , and 150° – 152° . The unindexed peaks are certainly not from the ZnMnO₃ nor Li₂Zn_{1- δ} Mn_{3+ δ} O₈, and they are most likely from unknown impurities. We, hence, exclude these 2θ ranges for the following refinement, and deduced the most probable magnetic structure. Below 17 K, several superlattice reflections are detected which can be indexed by a magnetic wave vector of $\mathbf{q} = (\frac{1}{2}, \frac{1}{2}, 0)$. Parameters determined from the refinement are summarized in Tables I and II in Supplemental Material III [24]. Details are discussed later.

IV. DISCUSSION

A. Magnetic interactions

First, we discuss the magnitude of the magnetic interactions in MgMnO₃ and ZnMnO₃. The Weiss temperature values of both compounds are very different: -43.8 and 3.96 K

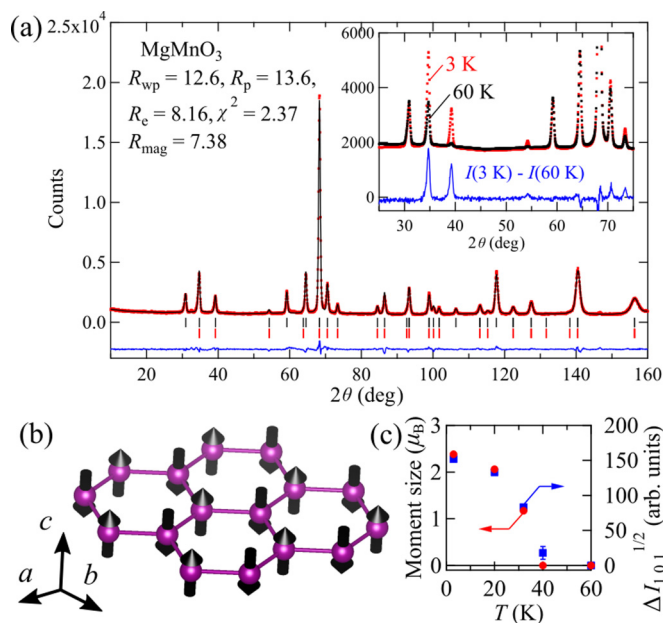


FIG. 8. (a) Neutron diffraction patterns of MgMnO_3 measured at 3 K. Red dotted, black solid, and blue solid curves indicate observed, calculated intensities, and their difference, respectively. Total neutron counts are 3.6×10^5 . Positions of nuclear and magnetic reflections for the Γ_3 irreducible representation are indicated by black and red bars, respectively. The observed intensities at 3 and 60 K are compared in the inset, together with their difference. Note that the observed intensities in the inset are shifted for 1000 counts for clarity. (b) Magnetic structure determined from the Rietveld refinement. Purple circles and black arrows indicate Mn atoms and magnetic moments, respectively. The figure is illustrated using the VESTA program [17]. (c) The magnitude of the magnetic moment estimated from the refinement and the square root of the integrated intensity from $1\ 0\ 1$ reflections $\Delta I_{101}^{1/2} = \sqrt{I_{101}(T) - I_{101}(60\text{ K})}$ plotted as a function of the temperature.

for MgMnO_3 and ZnMnO_3 , respectively. For MgMnO_3 , the transition temperature and the saturation field have a similar energy scale. Thus, competition between J_1 and J_2 should not be so strong. On the other hand, for ZnMnO_3 , the Weiss temperature is close to zero, indicating the coexistence of comparable ferromagnetic and antiferromagnetic interactions. To confirm these expectations, we roughly estimate the value of $\alpha = J_2/|J_1|$ from a ratio between a Weiss temperature θ_W and a saturation field $\mu_0 H_s$. The Weiss temperature and the saturation field are derived as a function of J_1 and J_2 from a mean field approximation. Then we take the ratio $-\theta_W/(\mu_0 H_s)$ since it only depends on the single parameter, $\alpha = J_2/|J_1|$. α is estimated as 0.13 (MgMnO_3) and 0.44 (ZnMnO_3) from $-\theta_W/(\mu_0 H_s)$ of 0.52 and -0.20 , respectively. Magnetic interactions to third and further nearest neighbors are not taken into account since its exchange path (Mn-O-Mg/Zn-O-Mn) has a long distance. The details are described in the Supplemental Material [24].

Next, we discuss the consistency of α from the viewpoint of the crystal structure. J_1 should be composed of two contributions: the ferromagnetic superexchange interactions J_s via a $\text{Mn}^{4+} - \text{O}^{2-} - \text{Mn}^{4+}$ path, and the antiferromagnetic direct exchange interactions J_d . According

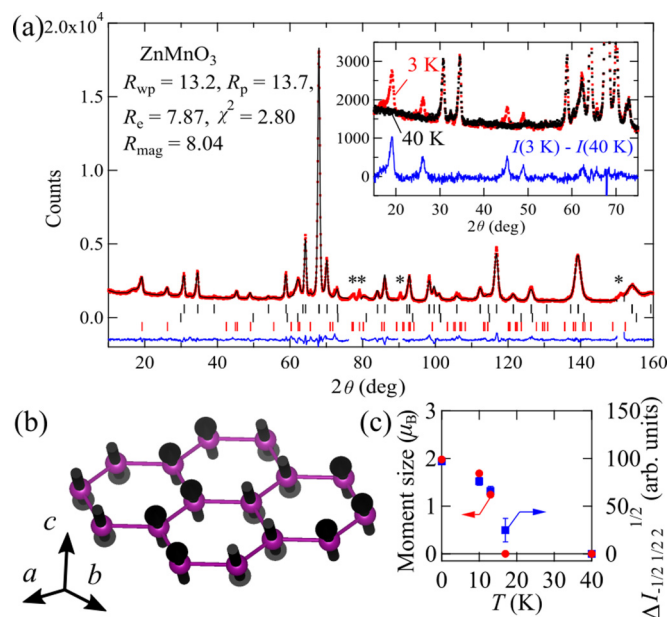


FIG. 9. (a) Neutron diffraction patterns of ZnMnO_3 measured at 3 K. Red dotted, black solid, and blue solid curves indicate observed, calculated intensities, and their difference, respectively. Total neutron counts are 3.6×10^5 . Positions of nuclear reflections expected for the main and secondary phases are indicated by top and middle black bars, respectively. Red solid bars indicate magnetic reflections expected for the Γ_2 irreducible representation. Asterisks indicate peaks from unknown impurities. The observed intensities at 3 and 40 K are compared in the inset, together with their difference. (b) Magnetic structure determined from the Rietveld refinement. Purple circles and black arrows indicate Mn atoms and magnetic moments, respectively. (c) The magnitude of the magnetic moment estimated from the refinement and the square root of the integrated intensity from $-\frac{1}{2}\ \frac{1}{2}\ 2$ reflections plotted as a function of temperature.

to the Kanamori-Goodenough rule, J_s is ferromagnetic at the bond angle close to 90° and becomes antiferromagnetic as the bond angle increases [29]. On the other hand, J_d should be antiferromagnetic because of finite overlap between d orbitals of neighboring magnetic ions [30]. Its magnitude decreases with increasing bond distance $d_{\text{Mn-Mn}}$ [31–33]. Since J_d is dominant for J_1 , magnetic interactions between two edge-sharing Mn^{4+}O_6 octahedra can change from antiferromagnetic to ferromagnetic as the bond distance increases. In fact, previous electron spin resonance studies of manganese spinel oxides confirmed that the $\text{Mn}^{4+} - \text{Mn}^{4+}$ coupling in two edge-sharing MnO_6 octahedra changes from antiferromagnetic to ferromagnetic at $d_{\text{Mn-Mn}} \sim 2.85 - 2.87 \text{ \AA}$ [34]. Let us recall that the nearest neighbor Mn-Mn bond distances are 2.8630(4) and 2.8741(5) \AA , respectively, for MgMnO_3 and ZnMnO_3 . Based on this distance, J_1 should be antiferromagnetic (ferromagnetic) in MgMnO_3 (ZnMnO_3). Then, J_2 of ZnMnO_3 should be antiferromagnetic since the Weiss temperature is zero. In addition, it is reasonable to assume that J_2 of MgMnO_3 is also antiferromagnetic owing to the super-superexchange path being similar to that of ZnMnO_3 . In summary, bond distances and magnetic properties of both compounds indicate antiferromagnetic J_1 and J_2 for

MgMnO_3 and ferromagnetic J_1 and antiferromagnetic J_2 for ZnMnO_3 .

B. Magnetic structure

The difference in exchange constants for both compounds is also supported by the magnetic structures at low temperatures. First, let us discuss the magnetic structure of MgMnO_3 . To determine the magnetic structure through the Rietveld refinement, first, candidates for initial magnetic structures of MgMnO_3 are obtained using magnetic representation theory [35]. The calculations were carried out using the software BASIREPS [36]. For MgMnO_3 , magnetic representations for the Mn moments are decomposed using the irreducible representations (IRs) of the k group with $k = (0, 0, 0)$, which is the same as the original space group $R\bar{3}$. The result of the decomposition is

$$\Gamma = \Gamma_1 + 2\Gamma_2 + \Gamma_3 + 2\Gamma_4, \quad (2)$$

and corresponding magnetic basis vectors (BVs) for all the IRs were obtained. Note that only two Mn ions ($z = 0.1608$ and 0.8392 at low temperatures) are present in a primitive rhombohedral lattice, and thus the BVs are categorized by a relation between the magnetic moments on the two ions. The BVs for Γ_1 and Γ_2 IRs describe a ferromagnetic order with c (Γ_1) and ab -spin components (Γ_2), whereas BVs for Γ_3 and Γ_4 describe a staggered Néel order with c - (Γ_3) and ab -spin components (Γ_4). The best fit is achieved using a single Γ_3 representation as shown in Fig. 8(a). The refined structure is illustrated in Fig. 8(b). Magnetic moments align in an antiparallel manner between the nearest neighbors in a single Mn layer. The layer is stacked along the c axis due to the translational symmetry of a rhombohedral lattice. The diffraction patterns measured at other temperatures are also fitted well by the same model (see Supplemental Material [24]). The magnitudes of the magnetic moments and the integrated intensity of 101 reflection are plotted as a function of a temperature in Fig. 8(c). The magnitude of magnetic moments at 3 K is estimated as $2.527(18) \mu_B$. With increasing temperatures, the magnitude of magnetic moments decreases and becomes undetectable at 40 K. The diffraction patterns at 3, 20, and 32 K exhibit very few differences except for the magnitude of the magnetic moment, indicating that the variation of the magnetic structure across T_a should be very small. In summary, the Rietveld analysis on the neutron powder diffraction pattern revealed that MgMnO_3 exhibits a Néel-type antiferromagnetic order.

Note that a ferrimagnetic order supported by the magnetization measurements requires additional Γ_1 or Γ_2 components. Since the magnetic order should be characterized by a single irreducible representation below a second-order phase transition in the framework of the Landau-Lifshitz theory, this requirement would indicate that the crystal symmetry is lowered from $R\bar{3}$. However, the fit converges very well only by a single staggered antiferromagnetic component, and the ferromagnetic component is about three orders of magnitude smaller than the moment size, as shown in Fig. 9. Thus, the structural distortion to lower the symmetry, even if it exists, should be so small that they cannot be detected in our powder

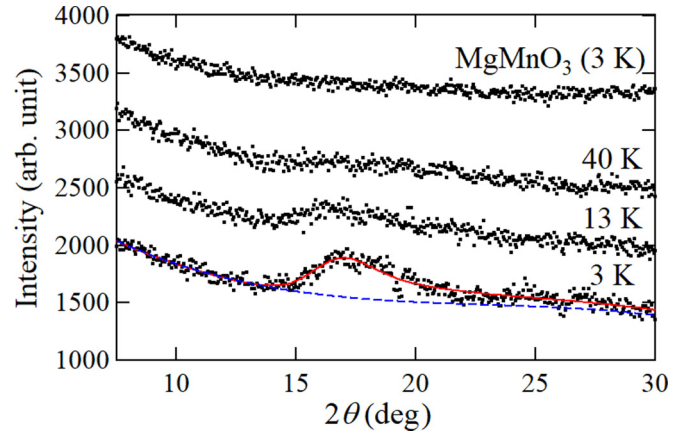


FIG. 10. Neutron diffraction patterns of MgMnO_3 and ZnMnO_3 after magnetic and nuclear reflections are subtracted. A red solid curve represents a diffuse scattering expected for a disordered layered system. A blue dashed curve corresponds to the expected background. Diffraction patterns measured at 13 and 40 K, and that of MgMnO_3 (3 K) are shifted for clarity.

diffraction experiments. This way, two inequivalent Mn sites may be induced by the lowered crystal symmetry.

On the other hand, a zigzag antiferromagnetic order is revealed for ZnMnO_3 from the diffraction pattern shown in Fig. 9(a). By decomposing reducible magnetic representations using IRs of the k group with $q = (\frac{1}{2}, \frac{1}{2}, 0)$, we found

$$\Gamma = 3\Gamma_1 + 3\Gamma_2, \quad (3)$$

and corresponding BVs representing a striped and zigzag antiferromagnetic structure for Γ_1 and Γ_2 IRs, respectively. The small ferromagnetic component indicated by the magnetization curve is too small to be detected in the powder diffraction pattern and good convergence is obtained only by a fit based on the Γ_2 representation. The refined structure is illustrated in Fig. 9(b). Magnetic moments indicate the same direction along a zigzag chain along the $\langle 110 \rangle$ direction, while nearest neighbor zigzag spin chains indicate the opposite direction. The fit yields the moment size of $1.979(25) \mu_B$. Its magnitude is smaller than $3 \mu_B$ expected for $S = 3/2$, likely due to disorder of a magnetic structure as described in the next paragraph. The magnetic moment is tilted from the c axis to the ab plane for $28.3(28)^\circ$, and its projected axis on the ab plane forms an angle of $54.3(27)^\circ$ from the a axis. With an increasing temperature, the tilting angle of the magnetic moments does not change so much, even near T_a of 7 K. The moment size diminishes to zero at 17 K, supporting the T_N of 17 K as shown in Fig. 8(c).

We here mention that a broad hump becomes prominent below T_N , in addition to the sharp Bragg peaks, as shown in Fig. 10. Although the peak is so broad and asymmetric that the profile function used for other reflections cannot be applied, its profile can be reproduced by that of a disordered layered system [37]. This suggests that the magnetic order includes stacking faults between some honeycomb layers. The 2θ angle is 16.3° , where $-\frac{1}{2} \frac{1}{2} 0$ reflection can appear. For a structure without the stacking fault, $h k 0$ reflections are not allowed for the Γ_2 IR. This extinction is caused by magnetic moments between neighboring layers aligned in an antiparallel manner.

On the other hand, if the magnetic moments are randomly aligned between layers, an asymmetric peak can appear at $h k 0$ positions. The disorder may not be so strong that such broad and asymmetric features are not apparent for the other peaks. The magnetic Bragg peak with the asymmetric profile is also observed in 3R-delafossite compounds, such as $\text{Ag}_3\text{LiMn}_2\text{O}_6$ [38].

The difference of magnetic structures in MgMnO_3 and ZnMnO_3 , which is probed by the neutron diffraction study, is in accordance with the different spin models discussed in the previous section. The phase diagram of the classical J_1 - J_2 - J_3 honeycomb model is established by mean field approximation [39,40]. The J_1 - J_2 - J_3 honeycomb model can exhibit ferromagnetic order, Néel order, zigzag, and striped antiferromagnetic order in addition to the incommensurate spiral order. The Néel order in MgMnO_3 indicates that antiferromagnetic J_1 is dominant, which is also consistent with our rough estimate of $\alpha = 0.13$ ($J_1 > 0, J_2 > 0$). On the other hand, the zigzag antiferromagnetic order in ZnMnO_3 requires a ferromagnetic J_1 and antiferromagnetic J_2 , together with weakly antiferromagnetic J_3 . Our rough estimate of $\alpha = 0.44$ ($J_1 < 0, J_2 > 0$) is not in contradiction with this requirement. Moreover, in the J_1 - J_2 honeycomb lattice, it is theoretically predicted that exotic multiple- q magnetic structures, such as ripple, melon, and antimelon states, can be realized in the range of higher J_2/J_1 values [7,8]. Note that in MgMnO_3 , both J_1 and J_2 are antiferromagnetic, while in ZnMnO_3 , J_1 is ferromagnetic and J_2 remains antiferromagnetic. Owing to the sign difference of J_1 , and the relation between J_1 and the Mn-Mn bond distance, it may be possible to increase the absolute value of J_2/J_1 in the solid solution system

$\text{Mg}_{1-x}\text{Zn}_x\text{MnO}_3$: J_1 can be tuned from antiferromagnetic to ferromagnetic with keeping J_2 antiferromagnetic. We believe that this approach should result in the occurrence of the above-mentioned exotic magnetic structures.

V. SUMMARY

We have synthesized the frustrated J_1 - J_2 honeycomb lattice magnets MgMnO_3 and ZnMnO_3 via a topochemical route and investigated its crystal/magnetic structure, magnetism, and thermodynamic properties. Considering the relation between magnetic properties and crystal structure, it is revealed that both compounds are well described by a spin model of a frustrated J_1 - J_2 honeycomb antiferromagnet, which is strongly supported by the magnetic structures determined by neutron diffraction measurement. Particularly, ZnMnO_3 is the first realization of a honeycomb lattice magnet with ferromagnetic J_1 and antiferromagnetic J_2 . This finding suggests that it is possible to tune J_2/J_1 through the Mn-Mn bond distance in the ilmenite structure. In this sense, the ilmenite-type honeycomb lattice antiferromagnets with d^3 magnetic ions will provide us with a unique platform to study frustrated magnetism.

ACKNOWLEDGMENTS

This work was supported by Japan Society for the Promotion of Science (JSPS) KAKENHI (Fostering Joint International Research, Grant No. JP18KK0150), and the CORE Laboratory Research Program “Dynamic Alliance for Open Innovation Bridging Human, Environment and Materials of the Network Joint Research Center for Materials and Device.”

-
- [1] P. W. Anderson, *Mater. Res. Bull.* **8**, 153 (1973).
 - [2] R. Moessner and S. L. Sondhi, *Prog. Theor. Phys. Suppl.* **145**, 37 (2002).
 - [3] P. A. Lee, *Science* **321**, 1306 (2008).
 - [4] L. Balents, *Nature (London, UK)* **464**, 199 (2010).
 - [5] S. Katsura, T. Ide, and T. Morita, *J. Stat. Phys.* **42**, 381 (1986).
 - [6] S. Okumura, H. Kawamura, T. Okubo, and Y. Motome, *J. Phys. Soc. Jpn.* **79**, 114705 (2010).
 - [7] T. Shimokawa and H. Kawamura, *Phys. Rev. Lett.* **123**, 057202 (2019).
 - [8] T. Shimokawa, T. Okubo, and H. Kawamura, *Phys. Rev. B* **100**, 224404 (2019).
 - [9] O. Smirnova, M. Azuma, N. Kumada, Y. Kusano, M. Matsuda, Y. Shimakawa, T. Takei, Y. Yonesaki, and N. Kinomura, *J. Am. Chem. Soc.* **131**, 8313 (2009).
 - [10] M. Alaei, H. Mosadeq, I. A. Sarsari, and F. Shahbazi, *Phys. Rev. B* **96**, 140404(R) (2017).
 - [11] M. Matsuda, M. Azuma, M. Tokunaga, Y. Shimakawa, and N. Kumada, *Phys. Rev. Lett.* **105**, 187201 (2010).
 - [12] N. Onishi, K. Oka, M. Azuma, Y. Shimakawa, Y. Motome, T. Taniguchi, M. Hiraishi, M. Miyazaki, T. Masuda, A. Koda, K. M. Kojima, and R. Kadono, *Phys. Rev. B* **85**, 184412 (2012).
 - [13] G. Shirane, S. J. Pickart, and Y. Ishikawa, *J. Phys. Soc. Jpn.* **14**, 1352 (1959).
 - [14] K. Tsuzuki, Y. Ishikawa, N. Watanabe, and S. Akimoto, *J. Phys. Soc. Jpn.* **37**, 1242 (1974).
 - [15] B. L. Chamberland, A. W. Sleight, and J. F. Weiher, *J. Solid State Chem.* **1**, 512 (1970).
 - [16] Y. Haraguchi, C. Michioka, A. Matsuo, K. Kindo, H. Ueda, and K. Yoshimura, *Phys. Rev. Mater.* **2**, 054411 (2018).
 - [17] K. Momma and F. Izumi, *J. Appl. Crystallogr.* **44**, 1272 (2011).
 - [18] S. Lee, S. Choi, J. Kim, H. Sim, C. Won, S. Lee, S. A. Kim, N. Hur, and J.-G. Park, *J. Phys.: Condens. Matter* **24**, 456004 (2012).
 - [19] J. Rodríguez-Carvajal, *Physica B (Amsterdam)* **192**, 55 (1993).
 - [20] V. S. Hernandez, L. M. T. Martinez, G. C. Mather, and A. R. West, *J. Mater. Chem.* **6**, 1533 (1996).
 - [21] Y. Haraguchi, A. Matsuo, K. Kindo, and Z. Hiroi, *Phys. Rev. B* **98**, 064412 (2018).
 - [22] Y. J. Lee, S.-H. Park, C. Eng, J. B. Parise, and C. P. Grey, *Chem. Mater.* **14**, 194 (2002).
 - [23] P. Strobel, A. Ibarra-Palos, M. Anne, C. Poinignon, and A. Crisci, *Solid State Sci.* **5**, 1009 (2003).
 - [24] See Supplemental Material at <http://link.aps.org/supplemental/10.1103/PhysRevMaterials.3.124406> for the sample dependence, the estimation of spin model, and the detail of Rietveld refinement.

- [25] L. Néel, *Ann. Phys. (Leipzig)* **12**, 137 (1948).
- [26] A. Olariu, P. Mendels, F. Bert, B. G. Ueland, P. Schiffer, R. F. Berger, and R. J. Cava, *Phys. Rev. Lett.* **97**, 167203 (2006).
- [27] Y. Okamoto, H. Yoshida, and Z. Hiroi, *J. Phys. Soc. Jpn.* **78**, 033701 (2009).
- [28] H. Ueda, A. Matsuo, K. Kindo, and K. Yoshimura, *J. Phys. Soc. Jpn.* **83**, 014701 (2014).
- [29] J. Kanamori, *J. Phys. Chem. Solids* **10**, 87 (1959).
- [30] K. Motida and S. Míahara, *J. Phys. Soc. Jpn.* **28**, 1188 (1970).
- [31] P. K. Baltzer, P. J. Wojtowicz, M. Robbins, and E. Lopatin, *Phys. Rev.* **151**, 367 (1966).
- [32] H. Ueda and Y. Ueda, *Phys. Rev. B* **77**, 224411 (2008).
- [33] A. N. Yaresko, *Phys. Rev. B* **77**, 115106 (2008).
- [34] R. Alcántara, M. Jaraba, P. Lavela, J. L. Tirado, E. Zhecheva, and R. Stoyanova, *Chem. Mater.* **16**, 1573 (2004).
- [35] Yu. A. Izyumov and V. E. Naish, *J. Magn. Magn. Mater* **12**, 239 (1979).
- [36] J. Rodriguez-Carvajal, BASIREPS, <ftp://ftp.cea.fr/pub/l1b/divers/BasIreps>.
- [37] B. E. Warren, *Phys. Rev.* **59**, 693 (1941).
- [38] R. Kumar, T. Dey, P. M. Ette, K. Ramesha, A. Chakraborty, I. Dasgupta, R. Eremina, S. Tóth, A. Shahee, S. Kundu, M. Prinz-Zwick, A. A. Gippius, H. A. Krug von Nidda, N. Büttgen, P. Gegenwart, and A. V. Mahajan, *Phys. Rev. B* **99**, 144429 (2019).
- [39] E. Rastelli, A. Tassi, and L. Reatto, *Physica B (Amsterdam)* **97**, 1 (1979). Note that the phase diagram is established for a ferromagnetic J_1 . That for antiferromagnetic J_1 can be obtained by reversing all of the spins for the one of the sublattice, and signs for J_1 and J_3 simultaneously.
- [40] D. E. McNally, J. W. Simonson, J. J. Kistner-Morris, G. J. Smith, J. E. Hassinger, L. DeBeer-Schmitt, A. I. Kolesnikov, I. A. Zaliznyak, and M. C. Aronson, *Phys. Rev. B* **91**, 180407(R) (2015).